

Predicting highly correlated hydride-ion diffusion in SrTiO_3 crystals based on the fragment kinetic Monte Carlo method with machine-learning potential

Hiroya Nakata^{1, a)}

*Kyocera Corporation, Research Institute for Advanced Materials and Devices,
3-5-3 Hikaridai Seika-cho Soraku-gun Kyoto 619-0237, Japan.*

Oxyhydrides have drawn attention because of their fast ion conductivity and strong reducing properties. Recently, hydride ion migration in $\text{SrTiO}_{3-x}\text{H}_x$ oxyhydride crystals has been investigated, showing that hydride ion migration is blocked by slow oxygen diffusion. In this study, we investigate the hydride-ion migration mechanism using a kinetic Monte Carlo approach to understanding the relationship between the hydride and oxygen ions. The difficulties in applying the method to hydride and oxygen ion migration involve complex changes in the ionic migration barrier, which shifts dynamically depending on the characteristics of the surrounding hydride and oxygen ions. We can predict these complex changes using a machine-learning neural network model. The simulation can then be performed using this model to predict the temperature-dependent ionic-migration behavior. We found that our simulation results with respect to the activation barrier for hydride ion diffusion accorded well with those obtained by experiment. We also found that hydride ion migration is affected by slow oxygen diffusion and that oxygen diffusion is accelerated by changes in the ionic migration barriers. The parallel-processing efficiency of our proposed method was 84.92 % for our 1,000-CPU implementation, suggesting that the approach should be widely applicable to simulations of ionic migration in crystals at a reasonable computational cost.

I. INTRODUCTION

Ionic conductors are attracting great interest because of their potential use in many electronic devices such as batteries¹⁻⁴, superconductors⁵, photocatalytic devices⁶, and solid fuel cells^{4,7}. Recently, a number

of studies have investigated replacing a significant proportion of the hydride ions by oxide ions to form oxyhydrides⁸⁻¹⁵. Because of their fast ion conductivity and strong reducing properties, oxyhydrides have potential as effective charge carriers in traditional electrochemical applications¹⁶⁻¹⁹, and as catalysts for ammonia synthesis²⁰.

^{a)}Electronic mail: hiroya.nakata.gt@kyocera.jp

Significant efforts have been made toward understanding the experimental results for oxyhydride materials. The mobility of hydride ions has been measured for $\text{LaSrCoO}_3\text{H}_{0.70}$ via quasi-elastic neutron scattering²¹ and for $\text{La}_{2xy}\text{Sr}_{x+y}\text{LiH}_{1x+y}\text{O}_{3y}$ via impedance measurements.¹⁸ The kinetics of hydride ions in ABO_3 -type perovskite materials are particularly challenging because the materials have high conductivity, making impedance measurements difficult to apply.

Hydride ion mobility in SrTiFeO_3 has been measured²² but the experiments could not separate fully the hydride ion diffusion from the oxide anion diffusion, and the kinetics of the hydride ions were unclear. Hydride ion diffusion in $\text{ATiO}_{3-x}\text{H}_x$ could be observed via the exchange reactions with D^{13} , $\text{N}^{23,24}$, and F^{24} . The kinetics of H/D exchange have also been analyzed by quadrupole mass spectrometry²⁵.

Recently, Liu et al.²⁶ measured the self-diffusion coefficient for hydride ions by combining secondary ion mass spectrometry and a first-principles study, suggesting an activation barrier of around 0.30 eV. Although this experimental study partially explained hydride ion diffusion, both experimental and theoretical studies on this topic have been limited in comparison to those dealing with the diffusion of oxide anions. Oxygen migration in oxyhydride materials has also not

been investigated.

Theoretical approaches also have powerful tools for understanding hydride ion diffusion. Iwazaki et al.^{27,28} investigated the complex-defect electronic structure of H in $\text{BaTiO}_{3-\delta}$ and $\text{SrTiO}_{3-\delta}$, and with the simulation results suggesting that the hydride ions were trapped by V_O . Liu et al.^{29,30} investigated the formation and migration energy of H in the $\text{BaTiO}_{3-\delta}$ and K_2NiF_4 types of oxyhydrides, which revealed the electronic configuration of the hydride ions. This first-principles study suggested that the activation barrier for hydride ion diffusion is 0.17 eV for $\text{SrTiO}_{3-\delta}$ ²⁶ and 0.28 eV for $\text{BaTiO}_{3-\delta}$ ³⁰. Because the simulated activation barrier for hydride ions (0.17 eV) was less than that obtained by experiment (0.30 eV), it is suggested that the fast hydride ion migration is retarded by slow oxide anion diffusion. Although theoretical first-principles studies suggest that slow oxide anion diffusion can retard hydride ion migration, how the presence of oxide anions affects the kinetics of hydride ion diffusion is still unclear. Therefore, kinetic simulation of oxyhydride diffusion remains an interesting subject of investigation.

The kinetic Monte Carlo (kMC) method³¹⁻³³ can be used to predict long-time-scale ionic diffusion in crystals, where the ions jump into the nearest site according to experimentally obtained or simulated ac-

tivation barriers. The kMC method has been used to predict the kinetics of many types of ionic migration and chemical reactions such as yttria-stabilized zirconia^{34,35}, oxygen diffusion in doped ceria^{36,37}, various chemical reactions³⁸⁻⁴⁴, material diffusion⁴⁵⁻⁴⁹, electrochemical impedance⁵⁰, chemical catalysis⁵¹⁻⁵⁷, and crystal growth^{58,59}.

Recently, we proposed an efficient parallel-processing approach for predicting ionic diffusion with fragment-based kMC (FkMC)⁶⁰. The method has been applied to $\text{SrTiO}_{3-\delta}$ systems using a simple Manning model⁶¹ as a pilot test. The activation barrier of hydride ions found⁶⁰ did not accord with experimentally derived activation barriers²⁶, suggesting that the simple Manning model is inadequate for predicting ionic diffusion behavior in oxyhydrides. A major reason for the discrepancy may be attributed to inhomogeneous potentials, i.e., the previous simulation model did not consider the complex potential energy surface (PES) composed of both hydride and oxide ions. Inclusion of such a complex oxyhydride PES into the kMC method is not straightforward, making the kinetic analysis of oxyhydrides a challenging issue in terms of computational science.

The aim of this study is to develop a kMC model that can simulate complex ionic migration in crystals, with the method being applied to predicting the kinetics of hydride

and oxide ions in $\text{SrTiO}_{3-\delta}$ oxyhydrides. To achieve this, the activation barrier for each hydride and oxide ion is refined based on changes in potential energy.

Such a refinement of the activation barrier using potential energy differences has been proposed by Koettgen et al.³⁷, and the approach convincingly explains the ionic conductivity of doped ceria obtained by experiment. Our previous research⁶⁰ also follows the approach of Koettgen et al.³⁷, with the method being used to investigate the effect of Fe dopant on oxide ion diffusion in $\text{SrTiO}_{3-\delta}$. Here, we extend the FkMC approach to one based on machine learning (ML), i.e., FkMC-ML, in which the complex potential-energy landscape is modeled in terms of ML-derived potentials, and the kMC simulation is performed using these predicted changes in potential energy.

First, the original FkMC is reviewed briefly and its extension to ML-based potential correction is described in detail. Second, the kinetics of hydride ion migration are evaluated using the new FkMC-ML model and the differences between the original and the ML-corrected potentials are discussed. We also compare the evaluated activation barrier of hydride ion with those obtained by experiment²⁶ to demonstrate the validity of the proposed approach. Third, the diffusion coefficient for the oxide ions is evalu-

ated and the effect of H concentration on both hydride and oxide ions is discussed, with the aim of understanding the mechanism of ionic migration in oxyhydrides. Finally, the parallel-processing efficiency of FkMC-ML is evaluated to show the effectiveness of the approach.

II. THEORY AND METHOD

A. Summary of the FkMC method

The kMC method is described in detail elsewhere³¹⁻³³. Here, we briefly describe the kMC approach to simulating ionic diffusion. In the jump-diffusion kMC approach, the transition rate (k_i^j) from atom i to atom j can be estimated as

$$k_i^j = A \exp \left[-\frac{E_{ij}^\dagger}{RT} \right], \quad (1)$$

where E_{ij}^\dagger , R , T , and A are the activation energy, universal gas constant, temperature, and pre-exponential factor, respectively. Summing the respective transition rates gives an estimate of the total rate constant r^{tot} , expressed as

$$r^{\text{tot}} = \sum_i^{n^{\text{atom}}} \sum_j^{n_i^{\text{site}}} k_i^j, \quad (2)$$

where n^{atom} and n_i^{site} are the total number of target atoms in the system and number of nearest neighbor sites for atom i , respectively. For example, in the case of an oxide

ion in perovskite crystal, $n_i^{\text{site}} = 8$ for all oxygen sites. The transition probability from i to j (p_i^j) is given by

$$p_i^j = k_i^j / r^{\text{tot}}. \quad (3)$$

By iteratively selecting the transition from i to j based on the probability p_i^j , the position of target site i is updated. Likewise, the next $n + 1$ th step simulation time t_{n+1} can be obtained from current time t_n and the total rate constant in Eq. 2:

$$t_{n+1} = t_n - \frac{\ln(r')}{r^{\text{tot}}}, \quad (4)$$

where r' is uniform random number from zero to one.

Because the total number of events is $n^{\text{atom}} \times n^{\text{site}}$, the total rate constant r^{tot} increases cubically with the size of lattice. Therefore, the simulation time step $t_{n+1} - t_n$ cubically decreases, and the kMC approach will be limited to relatively small systems. To reduce the computational cost of kMC, several block separation schemes have been developed^{62,63}, aiming to achieve good parallel-processing efficiency. We have recently proposed an alternative type of parallelizable scheme involving atom-based fragmentation⁶⁰, where the transition rate is estimated for each atom i and the maximum

rate constant for an atom is defined as

$$r_i = \sum_{j \in n_i^{\text{site}}} k_i^j, \quad (5)$$

$$r^{\text{max}} = \max(r_i). \quad (6)$$

If we adopt dynamic renormalization⁶⁴, then the transition probability p_i^j in Eq. 3 can be reformulated as

$$p_i^j = \frac{r^{\text{max}}}{r^{\text{tot}}} \frac{k_i^j}{r^{\text{max}}}. \quad (7)$$

The transition event selection can then be partitioned into the selection of an atom with $r^{\text{max}}/r^{\text{tot}}$ and the selection of an event for the independent atom k_i^j/r^{max} . With this renormalization, several ions can be updated simultaneously, and the parallelization of kMC becomes easier⁶⁰. In this study, we extend this approach by adopting ML potential correction.

B. Modification of transition rate with ML potential correction

The key parameter for kMC simulation is the activation barrier E_{ij}^\ddagger from i to j defined in Eq. 1. In the case of oxide ion migration in a single SrTiO₃ crystal, the PES is almost flat, as shown by black line in Fig. 1(a), and no correction of the activation barrier of E_{ij}^\ddagger is required.

However, the flat PES case is quite rare, with the actual PES often being affected by

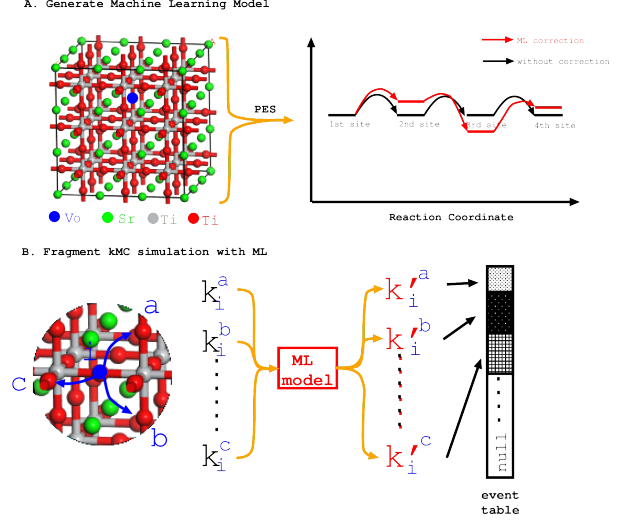


FIG. 1. A: schematic illustration of the effect of PES correction using the ML model. B: schematic illustration integrating the ML model into kMC simulation.

the presence of other types of ions. The main idea in this study is to consider correcting PES changes by using an ML model (the red line in Fig. 1(a)). The transition rate k_i^j can then be reformulated as

$$k_i^{j'} = A \exp \left[-\frac{E_{ij}^\ddagger + \Delta E_{ij}^{\text{ML}}/2}{RT} \right], \quad (8)$$

where $\Delta E_{ij}^{\text{ML}}$ is the potential energy difference between the final and the initial vacancy sites, which can be estimated via the ML model. A similar reformulation of the transition rate can be found in the recent review of Koettgen et al.³⁷.

As an example, for the case of a vacancy transition in an SrTiO₃ perovskite-type crystal, the vacancy can jump to any of the

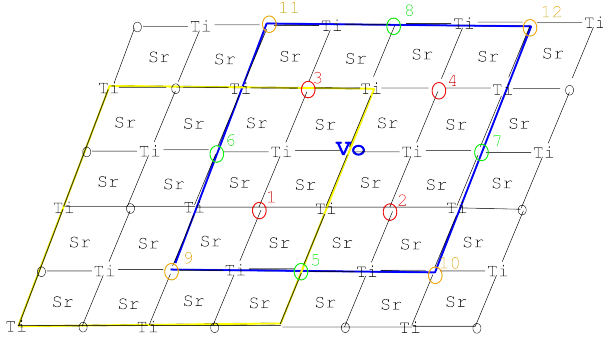


FIG. 2. Schematic illustration of constructing the feature vector for oxygen vacancy V_O , with colored labels 1, 2, 3, \dots indicating the elements of the feature vector.

eight nearest-neighbor sites (see Fig. 1(b), and Fig. 2). First, the transition rates from i to the other sites (a, b, \dots, c) are set from a pre-defined simulation parameter. The transition rate k_i^a is then refined using the ML model

$$\Delta E_{ij}^{\text{ML}} = f^{\text{ML}}(\mathbf{X}), \quad (9)$$

where f^{ML} is the ML model and \mathbf{X} is the feature vector used to predict $\Delta E_{ij}^{\text{ML}}$. In this study, the training of the ML model is aimed at developing the structure–energy relationship, with the energy being estimated using first-principles simulation.

The feature vector is a one-dimension array that represents the atomic configuration in the crystal. To show how the vector X is prepared, an example is shown in Fig. 2). In this example, we are trying to construct the feature vector for oxygen vacancy V_O , depicted in blue. The original position of V_O is

at the right edge of the periodic boundary condition (PBC) (the yellow line in Fig. 2). We apply the minimum-image convention for V_O and the PBC lattice is shifted to the blue line to locate the V_O at the center of the PBC (see Fig. 2). The atoms in the oxygen site are then reordered as the first nearest neighbor (red), the second nearest neighbor (green), and the third nearest neighbor (orange). They are labeled down to up and left to right (1, 2, 3, \dots 10 in Fig. 2). Using this labeling by the minimum image convention, the feature vector X can be filled for any atomic species. In the case of SrTiO_3 perovskite-type crystal, all the oxygen sites are symmetrical, making it possible to use a single ML model f^{ML} to predict the potential energy difference $\Delta E_{ij}^{\text{ML}}$. By inserting Eq. 9 into Eq. 8, $k_i^{j'}$, r_i , and r^{max} can be updated and the transition probability p_i^j can be updated using Eq. 7.

III. COMPUTATIONAL DETAILS

As noted in the Introduction, we investigated the kinetics of hydride and oxygen ions with the aim of understanding how the hydride and oxygen ions interact with each other. To achieve this, the FkMC-ML method was evaluated for four different levels of hydride ion concentration, namely for $\text{SrTiO}_{2.75}\text{H}_{0.25}$, $\text{SrTiO}_{2.65}\text{H}_{0.35}$,

and $\text{SrTiO}_{2.55}\text{H}_{0.45}$, and $\text{SrTiO}_{2.55}\text{H}_{0.60}$. The same concentrations of hydride ions (from 0.25 to 0.45) were used in the experimental study of Liu et al²⁶, with the simulated activation barriers being compared with the experimental results. Although $\text{SrTiO}_{2.55}\text{H}_{0.60}$ was not used in those experiments, we included it to evaluate fully how the simulation results change with an increase in hydride ions. The FkMC-ML simulation involves two main steps. The first step is to construct the ML model using the structure–energy relation and the second step is performing the FkMC-ML simulation to predict diffusion coefficients.

To construct the ML model, a first-principles simulation (DFT) was performed using Quantum Espresso software^{65,66} with a Perdew-Burke-Ernzerhof functional^{67,68}. We used ultrasoft pseudopotentials⁶⁹ and the cutoff energy for the plane-wave basis set was taken to be 300 Ry. The default convergence criterion of 1.0D-4 a.u was used for the geometry optimizations, and the default convergence criteria 1.0D-6 a.u was used for the self-consistent field calculations of the electronic states. The system size of SrTiO_3 in the first-principles simulation was $3\times 3\times 3$ and the total number of atoms was 135. (More detailed information about constructing an ML model is given in the Results and Discussion section.) In this study, we used tensorflow⁷⁰ to

construct the neural network model, where the neural network contained four hidden layers of 36 neurons each. To prevent overfitting, Ridge regression (L2 normalization) was adopted, with a coefficient of 0.001.

In the second step, a kMC-ML simulation was performed to evaluate the diffusion coefficients of the hydride ion and oxygen ion for each of the four hydride ion concentrations ($\text{SrTiO}_{2.75}\text{H}_{0.25}$, $\text{SrTiO}_{2.65}\text{H}_{0.35}$, and $\text{SrTiO}_{2.55}\text{H}_{0.45}$, and $\text{SrTiO}_{2.55}\text{H}_{0.60}$). In this case, the simulation system size was $90\times 90\times 96$ (the size of simulation system is 100 nm) and 288,000,000 simulation steps were performed. To evaluate the apparent activation energies for the various hydride ion concentrations, the temperature range was set to 550 K, 600 K, 650 K, and 700 K, for which the diffusion coefficient was experimentally measured²⁶. The vacancy concentration was set to 0.1 %. The simulation was parallelized using 144 central processing units (CPUs).

The FkMC-ML approach was implemented within the kMC program (written in C++) and the program was parallelized by using a message-passing interface. (The FkMC-ML program is available free of charge from GitHub (<https://github.com/hiroyanakata/kMC.v02>)). The parallel-processing efficiency of the kMC-ML was evaluated for the

SrTiO_{2.75}H_{0.25} case, where the system size was 900×900×900 (at a resolution of about 350 nm), and the kMC-ML simulation was performed using 1,000,000 steps. The computational costs were evaluated for the cases of 108, 216, 432, 864, and 1,000 CPUs and the parallel-processing efficiency was evaluated.

IV. RESULTS AND DISCUSSION

A. Generating the ML model from the DFT dataset

The reference datasets for the ML model were prepared using a standard kMC simulation (i.e., without the ML potential correction) and 1,000 structures were randomly generated in the single kMC simulation run. The system size was 3×3×3 unit cells, as noted in the Computational Details section, and independent kMC simulations were performed for four SrTiO_{3-x}H_x cases, where x was 0.25, 0.35, 0.45, or 0.60. For each simulation, one or two oxygen atoms were replaced with vacancies, giving eight sets of kMC simulations. Note that the insertion of two oxygen vacancies is at a higher concentration than was used in the actual kMC simulations, but we used both one-vacancy and two-vacancy models for the ML dataset to include the effect of the repulsion potential

between vacancies. The size of the dataset for evaluating the structure–energy relation was 8,000 and, using this dataset, we constructed the ML model used to predict the PES in oxyhydrides.

To construct the ML model, the feature vector X in Eq. 9 is prepared using three steps. First, from the trajectory obtained by kMC, the selected transition event ($V \rightarrow O$, $V \rightarrow H$) from site i to site j is determined and the atomic labels are assigned using the minimum image convention with respect to the center of the V_O site (site i) (see the Theory and Method section for details). Second, the labels of the atomic species (O, V, H) are replaced by the integer array (0, 1, 2) to obtain the sequential integer vector $X = [1, 0, 0, 2, \dots, 2]$. To distinguish the transition event from the i to j site, we use the negative integer labels -1 and -2 for the initial i site and final j site, respectively. Finally, we introduce another integer labeling (using 1 and 2) to distinguish the hydride ion and oxygen ion transitions, with the transition label “1” or “2” being put at the top of the feature vector. The completed feature vector then becomes $X = [1, -1, 0, -2, 2, \dots, 2]$, which contains all the necessary information (reaction type, transition site positions, and surrounding atomic species) to determine the change in PES.

The comparison between the ML energy

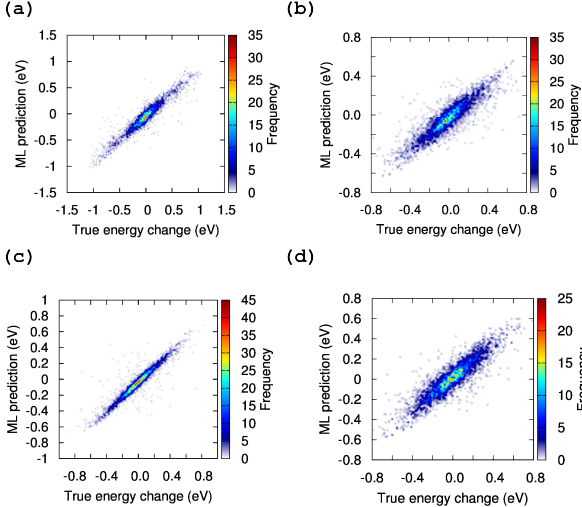


FIG. 3. Comparison between DFT energy (horizontal axis) and ML prediction energy (vertical axis). The colors show the numbers of data for each DFT energy: (a) the results for $\text{SrTiO}_{2.75}\text{H}_{0.25}$, (b) the results for $\text{SrTiO}_{2.65}\text{H}_{0.35}$, (c) the results for $\text{SrTiO}_{2.55}\text{H}_{0.45}$, and (d) the results for $\text{SrTiO}_{2.40}\text{H}_{0.60}$.

(energy predicted by the ML model) and the density functional theory (DFT) energy (energy estimated by the first-principles simulation) is depicted in Fig. 3. In Fig. 3, the horizontal axis represents the DFT energy and the vertical axis represents the predicted ML energy. The DFT energy denotes the energy difference in the ionic transition from the i site to the j site. As shown in Fig. 3, the ML model reproduces the DFT energy quite well and the root mean square error in Eq. 8 is 0.04 eV, which is less than the er-

ror expected for experimentally determined activation barriers²⁶. From Fig. 3, we note that the most of the DFT energies are located in a vicinity of zero, indicating that the PES is nearly flat. Furthermore, the comparison between ML and DFT energy shows a similar trend toward positive and negative changes in PES. These results suggest that the ML model developed is adequate for the kinetic simulation of oxyhydrides. We therefore adopt this ML model for predicting the diffusion coefficients of hydride and oxide ions in $\text{SrTiO}_{3-\delta}$.

B. Hydride ion diffusion coefficient evaluation using FkMC-ML

The hydride ion diffusion coefficients were evaluated for four oxyhydrides ($\text{SrTiO}_{3-x}\text{H}_x$, where $x=0.25, 0.35, 0.45,$ and 0.60), as noted in the Computational Details section. To evaluate the effect of ML correction on the diffusion coefficients, results for the standard kMC (i.e., without ML) were obtained and these results were compared with those obtained with the help of ML potentials. The results for the diffusion coefficients are shown in Fig. 4, where there is a significant difference between the diffusion coefficients obtained with and without the ML correction. For hydride ion concentrations of $x = 0.25$ or 0.35 , the PES accelerates the diffusion of

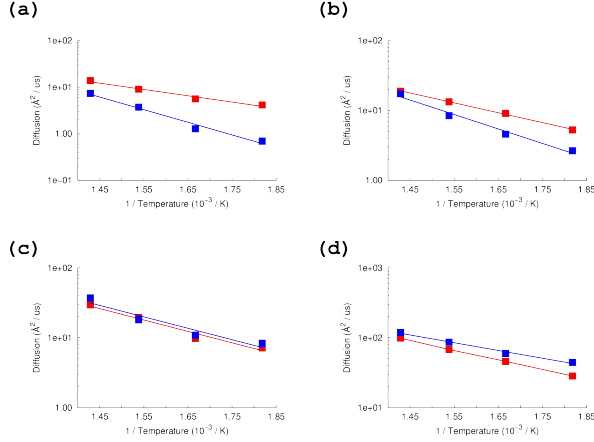


FIG. 4. The diffusion coefficient for hydride ions, with the red closed squares denoting the diffusion coefficients using kMC-ML, and the blue closed squares denoting those using kMC. The horizontal axis represents the inverse of temperature and the vertical axis represents the diffusion coefficients: (a) the results for $\text{SrTiO}_{2.75}\text{H}_{0.25}$, (b) the results for $\text{SrTiO}_{2.65}\text{H}_{0.35}$, (c) the results for $\text{SrTiO}_{2.55}\text{H}_{0.45}$, and (d) the results for $\text{SrTiO}_{2.40}\text{H}_{0.60}$.

hydride ions significantly, whereas the diffusion coefficient using kMC-ML remains the same for $x = 0.45$ and is slightly reduced for $x = 0.60$.

We can also note the difference in activation energy with and without PES correction. A summary of the activation barriers with and without ML correction is shown in Table I. Without the effect of PES correction, the activation barrier monotonically de-

creased with an increase in the concentration of hydride ions. The largest activation barrier was 0.53 eV for $x=0.25$, and the smallest was 0.27 eV. The changes of activation barriers can be understood in terms of slow oxygen diffusion. When the hydride ion concentration is small, the diffusion of hydride ions is limited by the surrounding oxygen ions. Therefore, the diffusion of hydride ions is affected by the oxygen ion concentration, with the activation barrier increasing with oxygen ion concentration. However, without PES correction, the estimated activation barriers are slightly larger than those obtained experimentally (See Table I). Inclusion of ML correction in Eq. 8 changes the activation barrier from 0.42 eV to 0.28 eV for $x = 0.35$ and this simulation result with ML correction agrees well with the experimentally derived activation barrier (0.28 eV). Likewise, for $x = 0.45$, the simulated activation barrier with ML is 0.32 eV, agreeing well with experiment (0.30 eV), which suggests that the simulation results are reasonable.

Note that the activation barriers estimated via FkMC-ML do not change very much with the variation of hydride ion concentration. However, without ML correction, the activation barrier is significantly changed, as noted above, indicating the importance of the ML potential contribution. For the case of $x = 0.25$, the activation barrier of

TABLE I. Apparent activation barrier for hydride ion diffusion in $\text{SrTiO}_{3-x}\text{H}_x$, for concentrations $x= 0.25, 0.35, 0.45,$ and 0.60 . ML and non-ML denote the results obtained by kMC-ML and standard kMC, respectively. N/A indicates that results are not available.

x	non-ML	ML	Liu et al. ²⁶
0.25	0.54	0.27	N/A
0.35	0.42	0.28	0.28
0.45	0.32	0.32	0.30
0.60	0.22	0.27	N/A

0.54 eV is close to the oxygen migration barrier in SrTiO_3 (0.6 eV), which suggests that the rate-determining step for hydride ions is oxygen migration. Using ML potentials decreases the barrier to 0.27 eV, which suggest that the inclusion of the PES may affect not only hydride ion migration but also oxygen ion migration, with both hydride and oxygen ion diffusion being accelerated. Because the hydride and oxygen ions interact significantly, the diffusion of oxygen should be analyzed to understand fully how hydride ion diffuse in SrTiO_3 crystals. We therefore also analyzed the kinetics of oxygen diffusion.

C. Oxygen ion diffusion coefficients

To understand fully the kinetics of SrTiO_3 oxyhydride, oxygen ion diffusion was also evaluated for the four hydride ion concen-

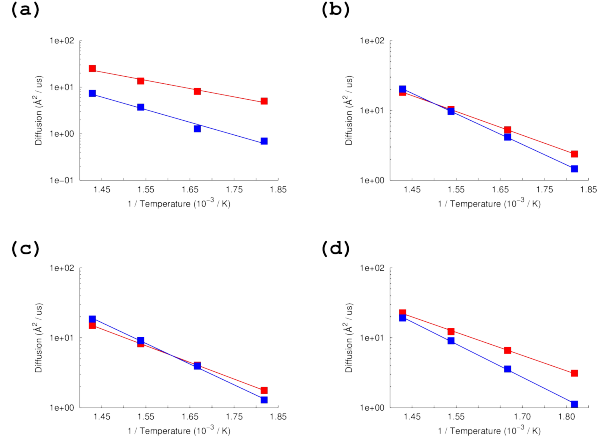


FIG. 5. The diffusion coefficient for oxygen ions, with the red closed square denoting the diffusion coefficients using kMC-ML, and the blue closed square denoting those using kMC. The horizontal axis is inverse of temperature, and the vertical axis represents the diffusion coefficients: (a) the results for $\text{SrTiO}_{2.75}\text{H}_{0.25}$, (b) the results for $\text{SrTiO}_{2.65}\text{H}_{0.35}$, (c) the results for $\text{SrTiO}_{2.55}\text{H}_{0.45}$, and (d) the results for $\text{SrTiO}_{2.40}\text{H}_{0.60}$.

trations. The results for the diffusion coefficients are shown in Fig. 5 and the activation energies are listed in Table II. Without PES correction, the activation barriers for oxygen ions do not depend on the concentration of hydride ions. The activation barriers are around 0.6 eV, which is the same as for oxygen migration in a single SrTiO_3 crystal.

Inclusion of the ML potential contribution changes significantly the kinetics of oxygen diffusion, particularly for small hydride

ion concentrations. When the hydride ion concentration is 0.25, the diffusion coefficient for oxygen using kMC-ML is ten times larger than that obtained without using ML potentials. The contribution of ML potentials to the diffusion coefficient is less noticeable when the simulation temperature is high, which is reasonable because the small changes in potential can be neglected given the increases from thermal fluctuation. Because of the temperature dependence, the apparent activation energy of oxygen ion diffusion decreases from 0.54 eV to 0.35 eV for $x = 0.25$. Similar trends can be observed in the simulation results for the other hydride ion concentrations, with the apparent activation energies being decreased by around 0.15 eV using the ML potential contributions for each hydride ion concentration.

TABLE II. Apparent activation barrier for oxygen ion diffusion in $\text{SrTiO}_{3-x}\text{H}_x$, for concentrations $x=0.25, 0.35, 0.45$, and 0.60 . ML and non-ML denote the results obtained by kMC-ML and standard kMC, respectively.

x	non-ML	ML
0.25	0.54	0.35
0.35	0.58	0.45
0.45	0.59	0.47
0.60	0.63	0.43

D. Hydride and oxygen ion diffusion mechanisms

To help understand the diffusion of hydride and oxygen ions, the changes in the activation energy for changing concentrations of hydride ions are shown in Fig. 6. In this figure, the difference between the blue and red lines shows the impact of the PES correction, summarizing the impact of interactions between hydride and oxygen ions.

The activation barrier for oxygen ions is uniformly reduced by considering PES changes, with the activation energy being around 0.4 eV (see Fig. 6(b)). By contrast, with hydride ion diffusion, the effect of PES correction does depend on the concentration of hydride ions. There is a reduction in activation energy for small hydride ion concentrations ($x = 0.25$ or 0.35), whereas the activation energy of the hydride ions remains similar for a higher hydride ion concentration ($x = 0.45$).

At a low hydride ion concentration ($x = 0.25$), hydride ions cannot diffuse without involving the diffusion of oxygen ions. Because the estimated oxygen diffusion is accelerated when considering ML potentials, the estimated diffusion of hydride ions will also be accelerated significantly. For a moderately high hydride ion concentration ($x = 0.35$ or 0.45), hydride ions can diffuse while interact-

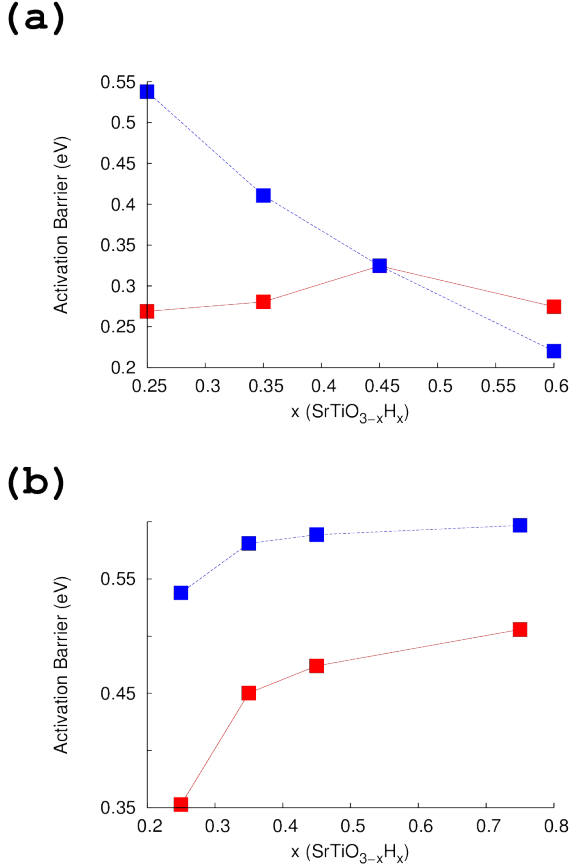


FIG. 6. Activation barriers for hydride ions in $\text{SrTiO}_{3-x}\text{H}_x$, for concentrations $x = 0.25, 0.35, 0.45$, and 0.6 . The red closed squares denote the diffusion coefficients using kMC-ML and the blue closed squares denote those using kMC: (a) the activation barrier for hydride ion diffusion and (b) the activation barrier for oxygen ion diffusion.

ing mainly with other hydride ions. The activation barrier without considering ML potentials will then also become less dependent on the activation barriers for oxygen ions (0.42 eV or 0.32 eV), confirming that slow oxygen

diffusion is not the primary rate-determining factor in such cases. Therefore, considering the decreased oxygen activation barrier by using ML potentials does not significantly affect the activation barriers for hydride ions. Likewise, at a high hydride ion concentration ($x = 0.60$), a decreased oxygen activation barrier would not accelerate hydride ion diffusion. In contrast to the other cases, using the ML potentials suppresses the diffusion of hydride ions, and the activation barrier is observed to increase from 0.22 eV to 0.27 eV. In summary, the activation barrier for hydride ions is around 0.3 eV, independent of the hydride ion concentration.

In this section, we have investigated the hydride and oxygen ion diffusion mechanisms by analyzing the activation barriers' dependence on the hydride ion concentration. Considering the inhomogeneous PES created via with ML model, the simulation results concur with the experimental activation barriers obtained by Liu et al.²⁶ (see Table I). This offers an insight into why the experimentally determined activation barrier does not depend on the hydride ion concentration. The simulation results indicate that there are two factors determining hydride ion diffusion, namely that increasing the concentration of hydride ions accelerates hydride ion diffusion and that using an inhomogeneous PES accelerates the diffusion of oxygen. These factors

affect the rate-determining step, particularly at low hydride ion concentrations.

E. Parallel-processing efficiency

Finally, the parallel-processing efficiency of FkMC-ML was evaluated for various numbers of CPUs in the range of 64 to 1,000, as noted in the Computational Details section. The results are shown in Fig. 7. In the figure, the red line is the actual computation time, and the black line is the ideally parallelized performance. Ideally, the computational time should decrease as the number of CPUs increases. We obtained a parallel efficiency of 84.92 % using 1,000 CPUs in a comparison with the 108-CPU case. The effective parallel-processing efficiency (the ratio by which the program can be parallelized) was 99.979 %, suggesting that most aspects of the simulation had been parallelized.

V. CONCLUSIONS

In this study, we have investigated hydride and oxygen ion diffusion in SrTiO₃ oxyhydride crystals using a FkMC-based simulation. Experimentally obtained observations about the interaction between oxygen ion and hydride ion diffusion were also observed in our simulations, with our results concurring with the experimentally obtained activation

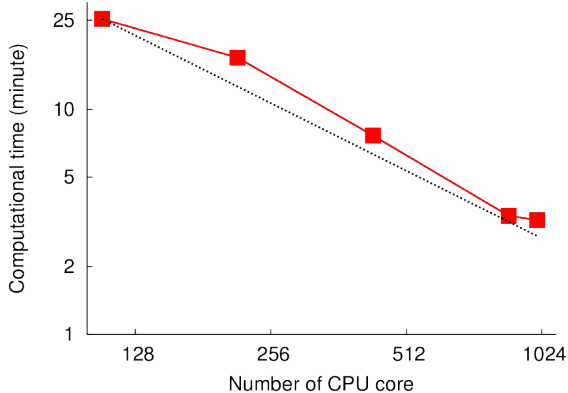


FIG. 7. Computational timing and its parallel-processing efficiency for FkMC-ML. The black dashed line is the ideal computational time, estimated by using the computational time with 64 cores.

barriers for hydride ion diffusion.

The FkMC simulation indicates that the activation barrier for hydride ions is affected by slow oxygen diffusion and that the estimates for oxygen diffusion rates are increased when considering an inhomogeneous PES. Therefore, the inclusion of such PES changes should be an important aspect of meaningful FkMC models.

In this study, we have developed an FkMC-based approach that includes neural-network capabilities, which enables the complex PES landscape to be included easily in the simulation model. The parallel-processing efficiency of the proposed approach is promising, suggesting that the approach can be widely used for simulating

ionic diffusion in crystals. We hope that our FkMC-ML simulation will aid the understanding of ion diffusion mechanisms in crystals.

ACKNOWLEDGMENTS

We thank the Research Institute for Information Technology at Kyushu University for providing computational resources. This research also used the computational resources of the Fujitsu PRIMERGY CX400M1/CX2550M5(Oakbridge-CX) at the Information Technology Center of the University of Tokyo through the HPCI System Research project (Project ID:hp200015).

REFERENCES

- ¹Y. Zhao, L. Xu, L. Mai, C. Han, Q. An, X. Xu, X. Liu, and Q. Zhang, *Proceedings of the National Academy of Sciences* **109**, 19569 (2012).
- ²J. Suntivich, H. A. Gasteiger, N. Yabuuchi, H. Nakanishi, J. B. Goodenough, and Y. Shao-Horn, *Nature chemistry* **3**, 546 (2011).
- ³N. Kamaya et al., *Nature materials* **10**, 682 (2011).
- ⁴L. Malavasi, C. A. Fisher, and M. S. Islam, *Chemical Society Reviews* **39**, 4370 (2010).
- ⁵Y. Kamihara, T. Watanabe, M. Hirano, and H. Hosono, *Journal of the American Chemical Society* **130**, 3296 (2008).
- ⁶M. I. Litter, *Applied Catalysis B: Environmental* **23**, 89 (1999).
- ⁷T. Ishihara, *Perovskite oxide for solid oxide fuel cells*, Springer Science & Business Media, 2009.
- ⁸A. Janotti and C. G. Van de Walle, *Nature materials* **6**, 44 (2007).
- ⁹S. Koch, E. Lavrov, and J. Weber, *Physical review letters* **108**, 165501 (2012).
- ¹⁰K. Hayashi, S. Matsuishi, T. Kamiya, M. Hirano, and H. Hosono, *Nature* **419**, 462 (2002).
- ¹¹G. Bouilly et al., *Chemistry of Materials* **27**, 6354 (2015).
- ¹²T. Yajima, A. Kitada, Y. Kobayashi, T. Sakaguchi, G. Bouilly, S. Kasahara, T. Terashima, M. Takano, and H. Kageyama, *Journal of the American Chemical Society* **134**, 8782 (2012).
- ¹³Y. Kobayashi et al., *Nature materials* **11**, 507 (2012).
- ¹⁴C. Tassel, Y. Goto, Y. Kuno, J. Hester, M. Green, Y. Kobayashi, and H. Kageyama, *Angewandte Chemie* **126**, 10545 (2014).
- ¹⁵C. Tassel et al., *Angewandte Chemie International Edition* **55**, 9667 (2016).
- ¹⁶Z. Zhang, Y. Zhu, Y. Zhong, W. Zhou, and Z. Shao, *Advanced Energy Materials* **7**,

- 1700242 (2017).
- ¹⁷S. Yamaguchi, *Science* **351**, 1262 (2016).
- ¹⁸G. Kobayashi, Y. Hinuma, S. Matsuoka, A. Watanabe, M. Iqbal, M. Hirayama, M. Yonemura, T. Kamiyama, I. Tanaka, and R. Kanno, *Science* **351**, 1314 (2016).
- ¹⁹Y. Yamazaki, F. Blanc, Y. Okuyama, L. Buannic, J. C. Lucio-Vega, C. P. Grey, and S. M. Haile, *Nature materials* **12**, 647 (2013).
- ²⁰Y. Kobayashi, Y. Tang, T. Kageyama, H. Yamashita, N. Masuda, S. Hosokawa, and H. Kageyama, *Journal of the American Chemical Society* **139**, 18240 (2017).
- ²¹C. A. Bridges, F. Fernandez-Alonso, J. P. Goff, and M. J. Rosseinsky, *Advanced materials* **18**, 3304 (2006).
- ²²S. Steinsvik, Y. Larring, and T. Norby, *Solid State Ionics* **143**, 103 (2001).
- ²³T. Yajima et al., *Nature Chemistry* **7**, 1017 (2015).
- ²⁴N. Masuda et al., *Journal of the American Chemical Society* **137**, 15315 (2015).
- ²⁵Y. Tang, Y. Kobayashi, K. Shitara, A. Konishi, A. Kuwabara, T. Nakashima, C. Tassel, T. Yamamoto, and H. Kageyama, *Chemistry of Materials* **29**, 8187 (2017).
- ²⁶X. Liu, T. S. Bjørheim, L. Vines, Ø. S. Fjellvåg, C. Granerød, Ø. Prytz, T. Yamamoto, H. Kageyama, T. Norby, and R. Haugrud, *Journal of the American Chemical Society* **141**, 4653 (2019).
- ²⁷Y. Iwazaki, T. Suzuki, and S. Tsuneyuki, *Journal of Applied Physics* **108**, 083705 (2010).
- ²⁸Y. Iwazaki, Y. Gohda, and S. Tsuneyuki, *APL Materials* **2**, 012103 (2014).
- ²⁹X. Liu, T. S. Bjørheim, and R. Haugrud, *Journal of Materials Chemistry A* **5**, 1050 (2017).
- ³⁰X. Liu, T. S. Bjørheim, and R. Haugrud, *Journal of Materials Chemistry A* **6**, 1454 (2018).
- ³¹C. Caron, editor, *An Introduction to Kinetic Monte Carlo Simulations of Surface Reactions*, Springer, Heidelberg in Germany, 2012.
- ³²G. Murch, *American Journal of Physics* **47**, 78 (1979).
- ³³K. E. Sickafus, E. A. Kotomin, and B. P. Uberuaga, *Radiation effects in solids*, volume 235, Springer Science & Business Media, 2007.
- ³⁴K. C. Lau, C. H. Turner, and B. I. Dunlap, *Chemical Physics Letters* **471**, 326 (2009).
- ³⁵K. C. Lau, C. H. Turner, and B. I. Dunlap, *Solid State Ionics* **179**, 1912 (2008).
- ³⁶S. Grieshammer, S. Eisele, and J. Koettgen, *The Journal of Physical Chemistry C* **122**, 18809 (2018).
- ³⁷J. Koettgen, S. Grieshammer, P. Hein, B. O. Grope, M. Nakayama, and M. Martin, *Physical Chemistry Chemical Physics* **20**, 14291 (2018).

- ³⁸S. Piccinin and M. Stamatakis, *ACS Catalysis* **4**, 2143 (2014).
- ³⁹C. Wu, D. Schmidt, C. Wolverton, and W. Schneider, *Journal of Catalysis* **286**, 88 (2012).
- ⁴⁰M. Stamatakis, Y. Chen, and D. G. Vlachos, *The Journal of Physical Chemistry C* **115**, 24750 (2011).
- ⁴¹L. Yang, A. Karim, and J. T. Muckerman, *The Journal of Physical Chemistry C* **117**, 3414 (2013).
- ⁴²W. Guo, M. Stamatakis, and D. G. Vlachos, *ACS Catalysis* **3**, 2248 (2013).
- ⁴³W. Guo and D. G. Vlachos, *Nature communications* **6**, 8619 (2015).
- ⁴⁴S. Lin, J. Ma, L. Zhou, C. Huang, D. Xie, and H. Guo, *The Journal of Physical Chemistry C* **117**, 451 (2013).
- ⁴⁵S. M. Auerbach, *International reviews in physical chemistry* **19**, 155 (2000).
- ⁴⁶S. Matera, H. Meskine, and K. Reuter, *The Journal of chemical physics* **134**, 064713 (2011).
- ⁴⁷B. Temel, H. Meskine, K. Reuter, M. Scheffler, and H. Metiu, *The Journal of chemical physics* **126**, 204711 (2007).
- ⁴⁸M. Rieger, J. Rogal, and K. Reuter, *Physical review letters* **100**, 016105 (2008).
- ⁴⁹R. Pornprasertsuk, T. Holme, and F. B. Prinz, *Journal of The Electrochemical Society* **156**, B1406 (2009).
- ⁵⁰R. Pornprasertsuk, J. Cheng, H. Huang, and F. B. Prinz, *Solid State Ionics* **178**, 195 (2007).
- ⁵¹E. W. Hansen and M. Neurock, *Chemical engineering science* **54**, 3411 (1999).
- ⁵²E. W. Hansen and M. Neurock, *Surface science* **464**, 91 (2000).
- ⁵³E. W. Hansen and M. Neurock, *Journal of Catalysis* **196**, 241 (2000).
- ⁵⁴K. Reuter and M. Scheffler, *Physical Review B* **73**, 045433 (2006).
- ⁵⁵M. Stamatakis, Y. Chen, and D. G. Vlachos, *The Journal of Physical Chemistry C* **115**, 24750 (2011).
- ⁵⁶J. A. Boscoboinik, C. Plaisance, M. Neurock, and W. T. Tysoe, *Physical Review B* **77**, 045422 (2008).
- ⁵⁷L. Kunz, F. M. Kuhn, and O. Deutschmann, *The Journal of chemical physics* **143**, 044108 (2015).
- ⁵⁸G. Gilmer, *Science* **208**, 355 (1980).
- ⁵⁹T. P. Schulze, *Journal of crystal growth* **263**, 605 (2004).
- ⁶⁰H. Nakata, *Computational Materials Science* **184**, 109844 (2020).
- ⁶¹J. R. Manning and L. Bruner, *AmJPh* **36**, 922 (1968).
- ⁶²K. Li, H. Shang, Y. Zhang, S. Li, B. Wu, D. Wang, L. Zhang, F. Li, D. Chen, and Z. Wei, *Openkmc: a kmc design for hundred-billion-atom simulation using millions of cores on sunway taihulight*, in *Pro-*

- ceedings of the International Conference for High Performance Computing, Networking, Storage and Analysis*, pages 1–16, 2019.
- ⁶³T. Tada and N. Watanabe, *ECS Transactions* **57**, 2437 (2013).
- ⁶⁴S. Grieshammer, B. O. Grope, J. Koettgen, and M. Martin, *Physical Chemistry Chemical Physics* **16**, 9974 (2014).
- ⁶⁵P. Giannozzi et al., *Journal of physics: Condensed matter* **21**, 395502 (2009).
- ⁶⁶P. Giannozzi et al., *Journal of Physics: Condensed Matter* **29**, 465901 (2017).
- ⁶⁷J. P. Perdew, J. A. Chevary, S. H. Vosko, K. A. Jackson, M. R. Pederson, D. J. Singh, and C. Fiolhais, *Physical review B* **46**, 6671 (1992).
- ⁶⁸J. P. Perdew, K. Burke, and M. Ernzerhof, *Physical review letters* **77**, 3865 (1996).
- ⁶⁹D. Vanderbilt, *Phys. Rev. B* **41**, 7892 (1990).
- ⁷⁰M. Abadi et al., *Tensorflow: A system for large-scale machine learning*, in *12th {USENIX} symposium on operating systems design and implementation ({OSDI} 16)*, pages 265–283, 2016.